Vasopressin excites interneurons to suppress hippocampal network activity across a broad span of brain maturity at birth

Albert Spoljaric[a,b,1], Patricia Seja[a,b,1], Inkeri Spoljaric[a,b], Mari A. Virtanen[a,b], Jenna Lindfors[a,b], Pavel Uvarov[a,b], Milla Summanen[a,b], Ailey K. Crow[c], Brian Hsueh[d], Martin Puskarjov[a,b], Eva Ruusuvuori[a,b], Juha Voipio[a], Karl Deisseroth[e,f,2], and Kai Kaila[a,b,2]

[a]Department of Biosciences, University of Helsinki, 00014 Helsinki, Finland; [b]Neuroscience Center, University of Helsinki, 00014 Helsinki, Finland; [c]CNC Program, Stanford University, Stanford, CA 94305; [d]Department of Bioengineering, Stanford University, Stanford, CA 94305; [e]Department of Bioengineering, Howard Hughes Medical Institute, Stanford University, Stanford, CA 94305; and [f]Department of Psychiatry, Howard Hughes Medical Institute, Stanford University, Stanford, CA 94305

Contributed by Karl Deisseroth, November 2, 2017 (sent for review October 6, 2017; reviewed by Colin Brown and Enrico Cherubini)

During birth in mammals, a pronounced surge of fetal peripheral stress hormones takes place to promote survival in the transition to the extrauterine environment. However, it is not known whether the hormonal signaling involves central pathways with direct protective effects on the perinatal brain. Here, we show that arginine vasopressin specifically activates interneurons to suppress spontaneous network events in the perinatal hippocampus. Experiments done on the altricial rat and precocial guinea pig neonate demonstrated that the effect of vasopressin is not dependent on the level of maturation (depolarizing vs. hyperpolarizing) of postsynaptic $GABA_A$ receptor actions. Thus, the fetal mammalian brain is equipped with an evolutionarily conserved mechanism well-suited to suppress energetically expensive correlated network events under conditions of reduced oxygen supply at birth.

KCC2 | bumetanide | oxytocin | birth asphyxia | GDP

In mammalian development, birth is an abrupt transitory stage, where dramatic physiological changes occur in all organ systems of the fetus to facilitate the adaptation of the neonate to extrauterine conditions (1). A major challenge for the brain, which relies on oxidative metabolism, is the period of obligatory asphyxia that is associated with the transition from umbilical to lung-based exchange of oxygen and carbon dioxide. In humans, various situations where this transition is protracted lead to pathophysiological perinatal asphyxia, with an annual global death rate of 4 million neonates (2) and a wide spectrum of psychiatric and neurological disorders among the survivors (3), underscoring the importance of studies on the basic physiological mechanisms that have evolved to protect the brain at and around birth. In the face of an energy metabolic crisis caused by lack of oxygen at birth, an obvious adaptive strategy to protect the brain is to suppress neuronal activity, especially in regions such as the neocortex and hippocampus, which are particularly sensitive to hypoxia.

Birth coincides with an exceptionally prominent activation of the fetal hypothalamus–pituitary–adrenal (HPA) axis, which plays a key role in adjusting cardiorespiratory, metabolic, and thermoregulatory functions, promoting the neonate's survival and protection of vulnerable organs against trauma during parturition (1, 4–9). Increased central drive of the fetal HPA axis at the level of both corticotropic and arginine vasopressin (AVP) signaling has been reported in late mammalian gestation and delivery (10). AVP, mainly derived from neurons located in the fetal hypothalamic supraoptic (SON) and paraventricular (PVN) nuclei (11, 12), is one of the key mediators of the birth-related adaptive stress responses (9, 10, 13, 14). During delivery, AVP secretion from the hypothalamic nuclei into the fetal circulation via the posterior pituitary is massively elevated (13–18). In sheep and humans (19–21), this parturition-related AVP surge has been shown to take place both in the blood and cerebrospinal fluid, further suggesting that central and peripheral vasopressinergic pathways are activated in parallel at birth. In the present context, it is of particular interest that hypoxia is an effective trigger of AVP release (13, 14, 18, 22), and that experimental neonatal asphyxia in the rat activates neurons in the PVN (23), which have central projections. It has been shown that in mature rodents, vasopressinergic fibers from the hypothalamus, particularly from the PVN, project to several limbic structures, including the entorhinal cortex, amygdala, and hippocampus (24–26), but such information on the perinatal brain is scarce (27). Finally, activation of V1a AVP receptors (V1aRs) has been shown to exert neuroprotective and antiinflammatory actions on neocortical and hippocampal neurons (28, 29).

As a whole, the above structural and functional data lay a promising foundation for a close examination of the possible perinatal actions of AVP in vulnerable neuronal networks. However, a challenge for studies on protective mechanisms is brought by the very different maturational level of the brain in distinct mammalian species at birth. For instance, the developmental

Significance

The transition from placental to lung-based oxygen supply at mammalian birth involves an obligatory period of asphyxia, which is further aggravated by complications during delivery. This oxygen deprivation is a major threat to the fetal brain, and, under such conditions, hormonal and cardiovascular mechanisms are activated to enhance brain perfusion. Our work now demonstrates an intrinsic mechanism in the fetal brain whereby vasopressin activates hippocampal interneurons, leading to desynchronization and suppression of neuronal network activity in species (rat and guinea pig) that are born at widely different stages of brain maturation. Silencing of synchronous neuronal activity by vasopressin is expected to decrease neuronal energy demand and prevent maladaptive synaptic plasticity, thus acting as a pan-mammalian neuroprotective mechanism during birth.

Author contributions: A.S., P.S., J.V., K.D., and K.K. designed research; A.S., P.S., I.S., M.A.V., J.L., P.U., M.S., A.K.C., B.H., M.P., and E.R. performed research; A.K.C. and K.D. contributed new reagents/analytic tools; A.S., P.S., I.S., M.A.V., J.L., P.U., A.K.C., B.H., M.P., and E.R. analyzed data; and A.S., P.S., M.P., E.R., K.D., and K.K. wrote the paper.

Reviewers: C.B., University of Otago; and E.C., SISSA, Trieste, Italy.

The authors declare no conflict of interest.

[1]A.S. and P.S. contributed equally to this work.

[2]To whom correspondence may be addressed. Email: deissero@stanford.edu or kai.kaila@helsinki.fi.

This article contains supporting information online at www.pnas.org/lookup/suppl/doi:10.1073/pnas.1717337114/-/DCSupplemental.

shift from depolarizing to hyperpolarizing $GABA_A$ receptor ($GABA_AR$)-mediated responses takes place postnatally in the rat but occurs already in the early fetal period in guinea pigs (30). A general mammalian neuroprotective mechanism at birth should be independent of whether GABA is depolarizing (i.e., rats) or hyperpolarizing (i.e., guinea pigs) in the neonate's brain.

In the present work, we provide evidence of powerful suppression of hippocampal spontaneous network events by AVP during the perinatal period. Our data show that at birth, the rat hippocampus is already innervated by vasopressinergic fibers. AVP at nanomolar concentrations leads to a V1aR-mediated transient suppression of spontaneous neuronal network activity in the perinatal hippocampus of both the altricial rat and the precocial guinea pig, independent of the maturational level of the GABAergic system. This suppression is caused by activation of CA3 stratum lucidum-radiatum (SLR) interneurons, leading to a decrease in the synchronous GABAergic activity that is needed for the sculpting of spontaneous network events paced by intrinsically bursting glutamatergic CA3 neurons (31–33). In sum, our work demonstrates a fast-acting mechanism whereby centrally released AVP is poised via suppression of energetically costly temporal overlap between GABAergic and glutamatergic synaptic inputs (34) to protect the perinatal brain during birth.

Results

Vasopressinergic Innervation of the Rat Hippocampus at Birth. While vasopressinergic innervation of the hippocampus has been demonstrated in adult rats (26), there are practically no structural data of this kind available for the newborn rat (27). Therefore, we combined the whole-tissue clearing method CLARITY (35) with immunostaining against neurophysin II (NPII; the AVP carrier protein) to specifically label vasopressinergic cells and projections (36). NPII-positive cell bodies were clearly seen in the PVN, SON, and accessory nuclei of the hypothalamus (Fig. 1 A_1 and A_2). In all samples, we detected segments of NPII-positive fibers scattered across the hippocampal formation (Fig. 1 B_1 and B_2, Fig. S1, and Movie S1). The NPII-positive fibers often appeared to be enriched in the vicinity of the hippocampal fissure, alveus, and fimbria. In addition, numerous NPII-positive fibers were detected in various parts of the limbic system, including the amygdala. These data indicate that the rat hippocampus receives vasopressinergic innervation at birth.

GABA Is Depolarizing Throughout the Perinatal Period. AVP is known to have a direct effect on a variety of neuronal populations (37). In the immature rat hippocampus in vitro, giant depolarizing potentials (GDPs), driven by depolarizing actions of GABA, represent the most prominent type of spontaneous network activity pattern (38). Thus, our next question was whether vasopressinergic signaling could modulate this early network activity at around birth. However, the depolarizing $GABA_AR$-mediated drive that GDPs depend on (31, 38, 39) has been suggested to be transiently abolished around birth by functional down-regulation of NKCC1 (40, 41). Hence, we first examined whether the NKCC1-dependent GDPs are present throughout the perinatal period [from embryonic day (E) 21.5 to postnatal day (P) 2]. Field GDPs (fGDPs), recorded from the CA3 region in the in toto hippocampal preparation (42), were reliably observed not only at P0 and later postnatal age points as described before (31, 39) but, in fact, throughout the perinatal period (Fig. 2 *A* and *B*). Notably, at all age points examined, fGDPs were completely blocked by the NKCC1 inhibitor

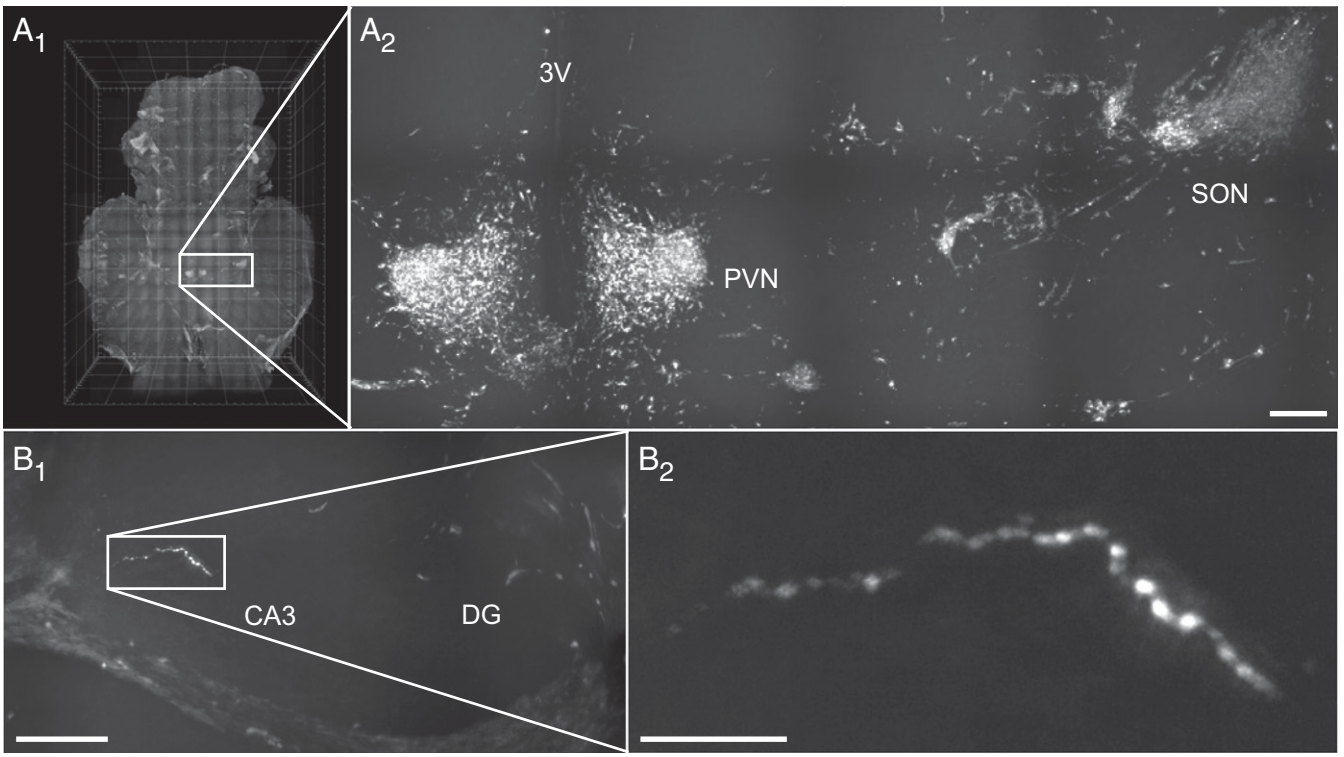

Fig. 1. Hippocampus of P0 rats receives vasopressinergic innervation. (A_1) Overview of a whole P0 rat brain optically cleared using CLARITY and stained against NPII ($n = 2$ within 2 h from birth and $n = 3$ during later time points at P0). Grid squares are 2 × 2 mm in size. (A_2) Rectangle in A_1 is shown at higher magnification. NPII staining strongly labels the vasopressinergic cell bodies in the hypothalamic area. The PVN are visible on the left side of the image, and the SON are visible in the upper right corner. 3V, third ventricle. (Scale bar: 200 μm.) (B_1) NPII-positive fibers were detected in various parts of the hippocampal formation, including CA3 and the dentate gyrus (DG). (Scale bar: 200 μm.) (B_2) Magnification of the rectangle shown in B_1 depicts a segment of a single NPII-positive fiber in the CA3 region. (Scale bar: 50 μm.) An overview of NPII-positive fibers throughout the hippocampus is shown in Movie S1.

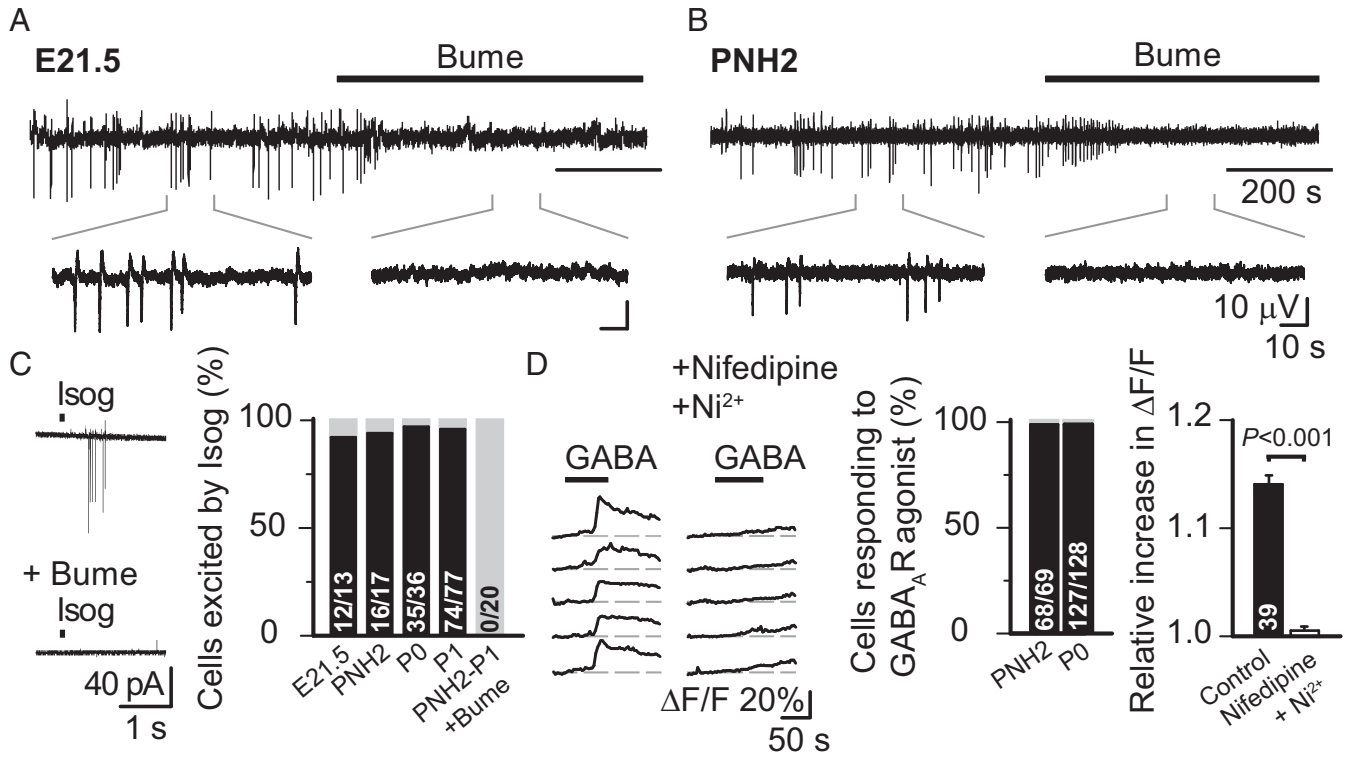

Fig. 2. GABA is depolarizing throughout the perinatal period in rat CA3 pyramidal neurons. Sample traces of fGDPs from the CA3 region of E21.5 (*A*) and PNH2 (*B*) in toto hippocampi (filtered at 1–10 Hz). Bumetanide (Bume, 10 μM) fully blocked fGDPs in all recordings (E21.5, $n = 3$; PNH2, $n = 5$). (*Insets*) Magnified views. (Scale bar values in *B* apply also to *A*.) (*C*) Puff-application of isoguvacine (Isog, 100 μM) elicits spiking in perinatal CA3 pyramidal neurons in the presence of iGluR block. Evoked spikes were abolished by bath application of Bume. Sample traces from a loose patch recording (*Left*) and the percentage of cells responding to Isog in all perinatal age groups (*Right*) are shown. (*D*, *Left*) Representative sample traces showing intracellular calcium $[Ca^{2+}]_i$ transients evoked by GABA (75 μM) in the absence and presence of the L- and T-type Ca^{2+} channel inhibitors nifedipine (10 μM) and Ni^{2+} (100 μM) in Fluo4-loaded CA3 pyramidal neurons. (*D*, *Center*) Percentages of cells responding to $GABA_AR$ activation with an increase in $[Ca^{2+}]_i$ at PNH2 and P0 . (*D*, *Right*) Mean reduction of $[Ca^{2+}]_i$ transients upon activation of $GABA_ARs$ before and during L- and T-type Ca^{2+} channel inhibition (pooled data from PNH2, $n = 19$; P0, $n = 20$; paired *t* test was used for statistical analysis). Data are provided as mean ± SEM, and *n* values are provided in bars. ΔF/F, fluorescence change divided by baseline fluorescence.

bumetanide (10 μM), indicating that GABA is depolarizing in the intact perinatal rat hippocampus.

To confirm that the perinatal excitatory GABA actions are present at the cellular level, we used both noninvasive loose cell-attached recordings and Ca^{2+} imaging in visually identified CA3 pyramidal neurons (Fig. 2 *C* and *D*). Puff-application of the selective $GABA_AR$ agonist isoguvacine (100 μM) elicited spiking in ∼95% of neurons (137 of 143 neurons) between E21.5 and P1 in the presence of ionotropic glutamate receptor (iGluR) blockers (*Materials and Methods* and Fig. 2*C*). The isoguvacine-evoked spiking was fully blocked by bumetanide. Here, we would like to point out that these experiments are not intended to address the question of whether $GABA_AR$ actions would directly evoke spikes in vivo (43, 44), but they do indicate that the reversal potential of $GABA_AR$-mediated current (E_{GABA}) is maintained by NKCC1-dependent Cl^- accumulation at a level more positive than the resting membrane potential. In agreement with the above observations, Ca^{2+} imaging done in CA3 pyramidal neurons from slices collected within 2 h after birth and during later time points at P0 showed that $GABA_AR$ activation (with either GABA or muscimol) evoked substantial intracellular Ca^{2+} transients in virtually all (195 of 197) cells (Fig. 2*D*). These Ca^{2+} transients were blocked by a combination of nifedipine (10 μM) and Ni^{2+} (100 μM), which act as antagonists of L- and T-type Ca^{2+} channels, respectively. Together, these results indicate that in hippocampal CA3 pyramidal neurons, GABA is depolarizing throughout the perinatal period.

AVP Suppresses Perinatal fGDPs via V1aRs. After confirming the presence of network activity driven by depolarizing GABA in the perinatal rat hippocampus, we moved on to test how it is affected by exogenous AVP. At 10 nM, AVP had a robust suppressing action on fGDPs recorded from the in toto rat hippocampus throughout the perinatal period (Fig. 3*A* and Fig. S2 *A* and *B*). This suppression was both qualitatively and quantitatively similar in hippocampal slices (Fig. S2*B*). In both preparations, the AVP-mediated suppression of fGDPs was transient, which is readily explained by receptor desensitization (45). Recovery from desensitization was near complete after 10 min of AVP washout as seen in experiments with two consecutive applications (Fig. S2*C*).

Central neurons are known to express V1aRs, V1bRs, and oxytocin receptors (OTRs) (37), and AVP is a potent ligand for each of them (46). Importantly, we found that the suppression of fGDPs by AVP was largely prevented by SR49059, a competitive antagonist (47) of V1aRs (Fig. 3*B*). At 20 nM, SR49059 is selective for V1aRs (K_i = 2.2 nM for V1aRs, K_i = 671 nM for V1bRs, and K_i = 76 nM for OTRs). As might be expected on the basis of the competitive nature of SR49059, the block of the action of AVP was not complete. Notably, however, SR49059 (20 nM) by itself did not affect fGDPs (Fig. S3). Since AVP has an almost equal affinity for V1aRs and OTRs in the rat (K_i at V1aR = 2.6 nM vs. K_i at OTR = 1.7 nM) (46), we tested whether OTRs play any role in the AVP-induced suppression of fGDPs. Unlike AVP, 10 nM oxytocin (OT) had no discernible effect on fGDPs (Fig. 3*C*). Given that the OT K_is for OTRs and V1aRs

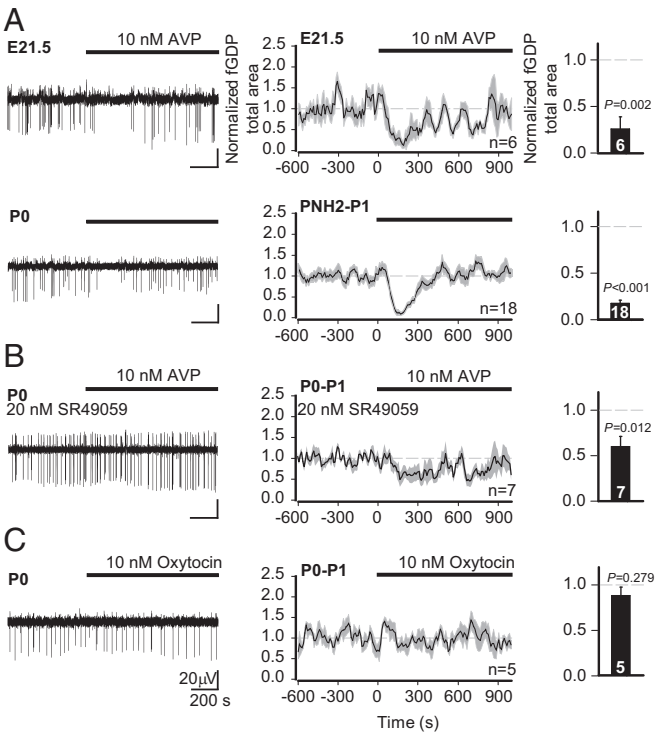

Fig. 3. AVP suppresses hippocampal fGDPs in a V1aR-dependent manner during the perinatal period. (*A–C, Left*) Sample traces of fGDPs measured from the hippocampal CA3 region (filtered at 1–10 Hz). (*A–C, Center*) Continuous quantification of the mean normalized fGDP total area throughout the experiment; data are shown as a moving average (60-s window, 10-s bins, 10-s step) ± SEM. (*A–C, Right*) Quantification of the neurohormone effect on the mean normalized fGDP total area (mean ± SEM). Here and in the following figures, we quantified the (average) values during minutes 2 to 4 from the start of AVP application. (*A*) Effect of AVP (10 nM) on fGDPs in E21.5 and PNH2–P1 in toto hippocampi. (*B*) AVP application in the continuous presence of the V1aR antagonist SR49059 in P0–P1 hippocampal slices. (*C*) fGDPs in P0–P1 slices before and during bath application of OT (10 nM). The *n* values are provided in the panels. A paired *t* test was used for statistical analysis. (Scale bar values in *C* apply to all sample traces.)

are 1.0 nM and 71 nM (46), respectively, the above observations show that the suppression of perinatal fGDPs by nanomolar AVP concentrations is mediated by V1aRs, with no involvement of OTRs.

GABAergic Input onto Pyramidal Neurons Is Increased by AVP. As the synchronous activation of both pyramidal neurons and interneurons has been shown to be crucial for the generation of fGDPs (31, 39), alterations in the excitability of either of these cell types could underlie the observed effect of AVP. Multiple-unit activity recorded extracellularly in CA3 stratum pyramidale (SP) in the presence of iGluR block and picrotoxin was not altered by application of AVP (Fig. S4*A*). Furthermore, neither pyramidal neuron spontaneous excitatory postsynaptic currents (sEPSCs) nor intrinsic properties (voltage-clamp recordings of holding current and current-clamp recordings of input resistance) were affected by AVP (Fig. S4 *B–D*). Together, these data show that the suppression of fGDPs by AVP is not mediated by direct modulation of the excitability of CA3 pyramidal neurons. Hence, we shifted our focus onto CA3 interneurons.

We recorded spontaneous inhibitory postsynaptic currents (sIPSCs) from pyramidal neurons in the presence of iGluR block. Strikingly, AVP (10 nM) increased the frequency of sIPSCs by about a factor of 2 (Fig. 4*A*). This increase was strongly attenuated in the presence of SR49059 (20 nM). In line with the effect of this antagonist in fGDP experiments (Fig. 3*B*), a small yet significant increase remained (Fig. 4*A*). The increase of sIPSC frequency was not markedly potentiated by using higher concentrations of AVP (Fig. 4*B*). Neither the amplitude of sIPSCs nor the frequency and amplitude of tetrodotoxin (TTX)-insensitive miniature IPSCs (mIPSCs) were affected by AVP (Fig. S5). Importantly, AVP had no effect on the driving force of $GABA_AR$-mediated currents in pyramidal neurons, as assessed in gramicidin-perforated patch recordings (Fig. S6). In conclusion, our data show that the increase in sIPSC frequency was due to increased spiking of interneurons and AVP did not affect pyramidal neuron properties.

AVP Specifically Activates SLR Interneurons via V1aRs. Next, we performed whole-cell current-clamp recordings from visually identified GABAergic interneurons in slices from P0–P2 VGAT-Venus rats (48) in the presence of iGluR block and picrotoxin (Fig. 4 *C–E* and Fig. S7). Upon application of AVP, the membrane potential of CA3 SLR interneurons depolarized by 4 ± 0.85 mV from a resting level of −59.9 ± 1.2 mV ($n = 7$), leading to a consequent increase in their spike frequency. Both the depolarization and the subsequent increase in the spike rate were prevented by SR49059 (Fig. 4 *C–E*). Notably, interneurons located in CA3 stratum oriens (SO) and SP did not respond to AVP (Fig. 4 *D* and *E* and Fig. S7).

To examine the expression of V1aRs in the CA3 area of the P0 rat hippocampus, we used the highly sensitive fluorescent in situ RNAscope assay (49). In agreement with our electrophysiological data, V1aR mRNA was detected in the SLR, where it localized to a subset of Gad1- and Gad2-positive interneurons (Fig. 4 *F* and *G*). In contrast, V1aR expression was low in SP and not detectable in SO. We did not detect V1bR mRNA in the P0 hippocampus (Fig. 4 *F* and *G*, a positive control is shown in Fig. S8). In conclusion, our data show that AVP specifically activates SLR interneurons via V1aRs in the CA3 area of the perinatal hippocampus.

AVP Suppresses fGDPs by Decreasing Synchronous GABAergic Drive. The synchronous activity of interneurons, promoting a depolarizing and excitatory GABAergic drive upon glutamatergic CA3 pyramidal neurons, plays a crucial role in the generation and temporal patterning of fGDPs (31, 33, 50). Therefore, tonic firing of interneurons, such as that triggered by AVP, is expected to interfere with the role of GABAergic signaling in network synchronization, thereby suppressing the fGDPs. To test this, we performed triple-electrode recordings with intracellular current- and voltage-clamp recordings from two CA3 pyramidal neurons (~100–200 μm apart) and a local field potential (LFP) electrode in the SP to monitor fGDPs (Fig. 5*A*). As is evident in the specimen recording, the robust and stable patterns of depolarization and firing of the pyramidal neurons (intracellular GDPs) were disrupted in the presence of AVP, which is in full agreement with the suppression of their extracellular network level counterparts, the fGDPs (Fig. 5*B*). In more quantitative terms, the rate of pyramidal spiking during GDPs was dramatically decreased by AVP (Fig. 5*C*). This decrease in "GDP-nested" spiking is not attributable to a general change in pyramidal neuron excitability (also Fig. S4), as the pyramidal neurons' inter-GDP spike rates remained unaffected by AVP (Fig. 5*C*). Moreover, GDP-associated synchronous GABAergic drive onto pyramidal neurons, as quantified by sIPSC burst area, was suppressed to about 50% from baseline levels (Fig. 5*D*). Additionally, the AVP-induced effects on sIPSC frequency and sIPSC burst total area displayed strikingly similar time courses (Fig. 5*D*). Together, these data support the idea that the loss of the synchronous excitatory drive of interneurons is the underlying mechanism by which AVP suppresses fGDPs in the neonatal rat hippocampus.

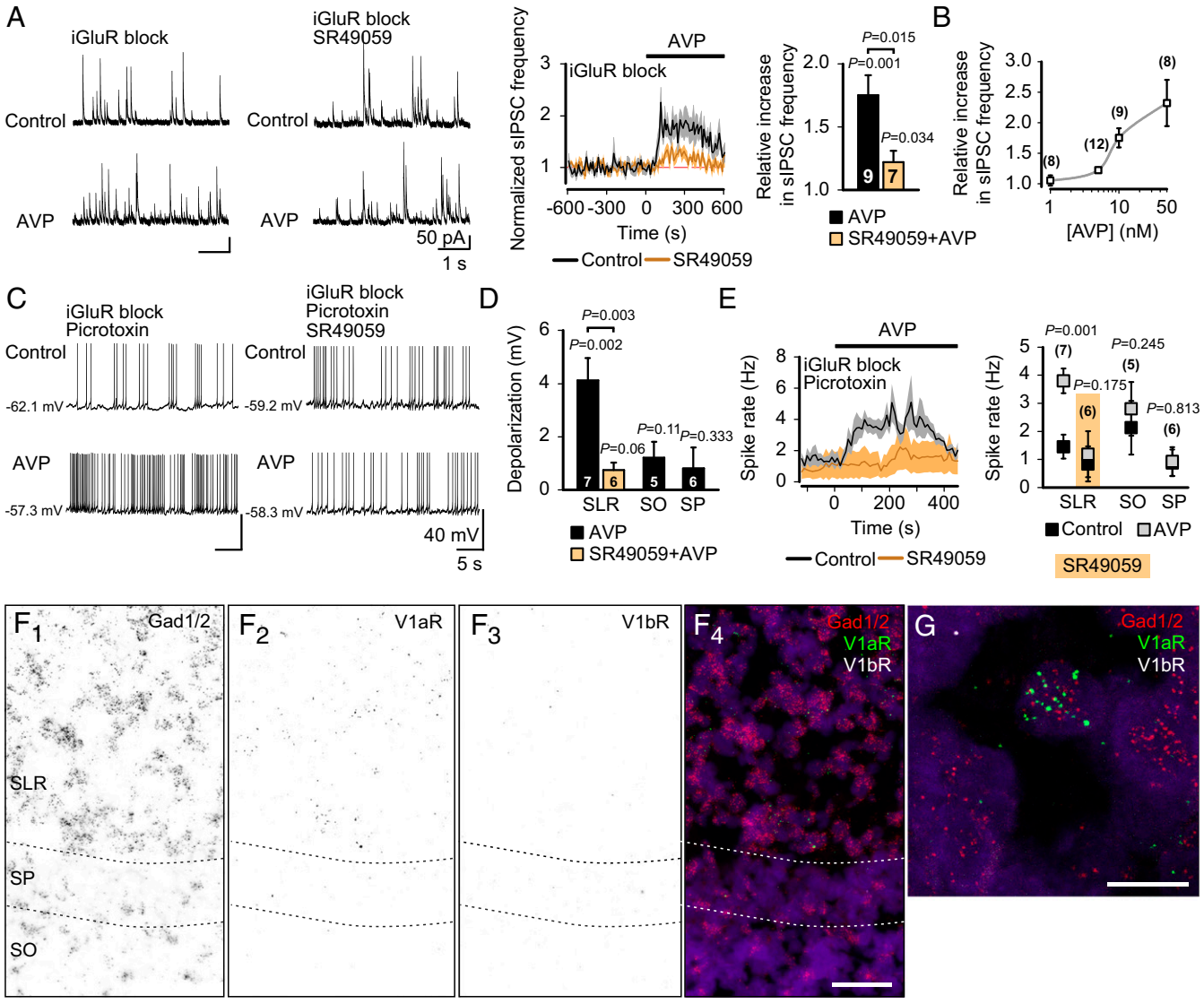

Fig. 4. AVP activates P0–P2 CA3 SLR interneurons via V1aRs. (*A*) Sample traces of whole-cell voltage-clamp recordings (*Left*) and mean normalized frequencies (*Center* and *Right*) of sIPSCs measured from CA3 pyramidal neurons before and during bath application of AVP (10 nM). AVP induced an increase in sIPSC frequency, which was significantly smaller in the presence of SR49059 (20 nM). (*B*) AVP concentration-response curve (1–50 nM) on normalized peak sIPSC frequency. (*C*) Whole-cell current-clamp recordings from visually identified hippocampal CA3 interneurons from P0–P2 VGAT-Venus transgenic rat slices before and during bath application of AVP (in the presence of iGluR block and picrotoxin). Sample traces of SLR interneurons in the absence (*Top*) and presence (*Bottom*) of SR49059 are shown. (*D*) Depolarization of interneurons from SLR (in the absence or presence of SR49059), SO, and SP upon application of AVP. (*E*, *Left*) Continuous quantification of the mean spike rate of SLR interneurons before and during bath application of AVP. (*E*, *Right*) Comparison of spike rates (control vs. peak effect of AVP) of interneurons from SLR (in the absence or presence of SR49059), SO, and SP before and during application of AVP. Data are presented as mean ± SEM, and *n* values are provided in the figure. Paired and independent *t* tests were used for statistical analysis. See Fig. S6 for additional data on SO and SP interneurons. (*F* and *G*) In situ hybridization with fluorescent probes against Gad1 and Gad2, V1aR, and V1bR mRNA transcripts in the CA3 region of the P0 rat hippocampus ($n = 5$ brains). (F_1) Gad1/2 mRNA black puncta label interneurons in all layers. (F_2) V1aR mRNA is predominantly expressed in the SLR. (F_3) V1bR mRNA expression was not detected in the CA3 area. (F_4) Merge of $F_{1–3}$. (Scale bar: 50 μM.) (*G*) Confocal image taken from the SLR. V1aR mRNA (green) localizes to a Gad1/2-positive cell (red). (Scale bar: 10 μm.) DAPI (purple) was used for nuclear staining. A positive control of the V1bR mRNA probe is shown in Fig. S7.

Suppression of Hippocampal Network Events by AVP Does Not Depend on the Level of Maturation of Neuronal Cl^- Extrusion. To study whether the desynchronizing action of AVP on hippocampal network events is dependent on the stage of maturation of Cl^- extrusion, we employed the guinea pig, a precocial species, whose young are born at a much more mature stage of cortical development (51). In contrast to the rat, guinea pig hippocampal pyramidal neurons express high levels of transport-functional KCC2 and generate robust hyperpolarizing $GABA_AR$ responses already by birth (30). In agreement with this, whole-cell recordings with a high somatic Cl^- load imposed via the patch pipette demonstrated robust KCC2-mediated Cl^- extrusion capacity in P0 guinea pig CA3 pyramidal neurons, similar to that seen in juvenile P16 rats (Fig. $6A_{1–3}$). In contrast, active Cl^- extrusion was virtually absent in both newborn rats and midgestation guinea pig embryos (Fig. $6A_3$). The temporal expression patterns of KCC2 protein in the rat and guinea pig hippocampus (Fig. 6*B*) fully complemented the results obtained in the measurements of Cl^- extrusion capacity, which is in line with the difference in the timing of brain development relative to birth in these two species (51).

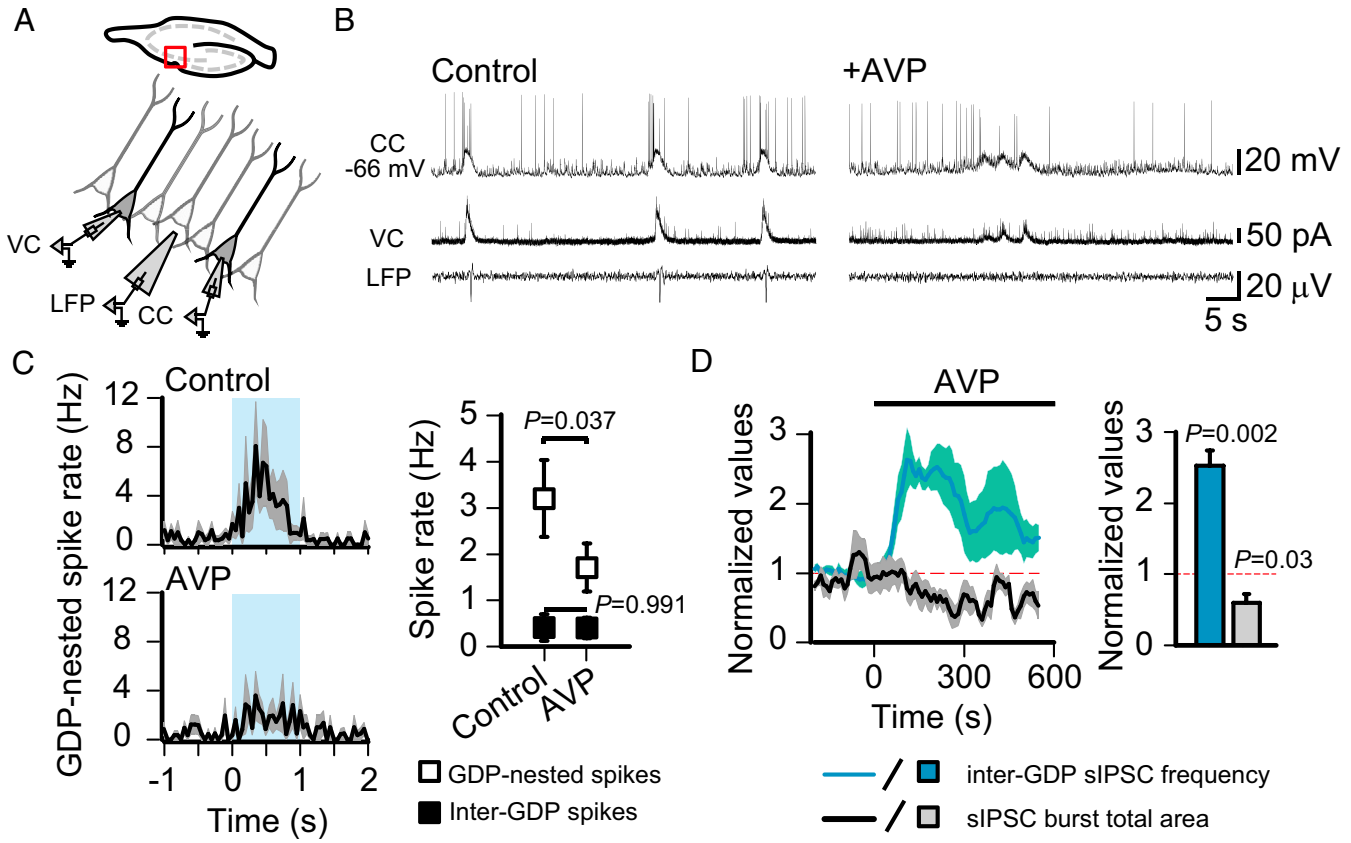

Fig. 5. AVP suppresses GDP-nested pyramidal neuron spiking by decreasing the synchronous GABAergic drive during network events. (*A*) Scheme of the triple-electrode recording from CA3 SP. CC, current clamp from a pyramidal neuron; VC, voltage clamp from a pyramidal neuron. (*B*) Sample traces before (*Left*) and during (*Right*) bath application of AVP (10 nM, $n = 5$ P0–P1 slices). LFP sample traces were filtered at 1–10 Hz. (*C*) Temporal distribution of pyramidal neuron spikes during GDPs (*Left*; control: 45 GDPs vs. AVP: 44 GDPs, bin size = 50 ms, the blue area indicates the 1-s time window from which the GDP-nested spikes were analyzed) and quantification of pyramidal neuron spike rates before and during application of AVP (*Right*). (*D*, *Left*) Mean normalized sIPSC burst total area before and during bath application of AVP. Mean normalized inter-GDP sIPSC frequency is shown for comparison. Data are shown as a moving average ± SEM. (*D*, *Right*) Bar diagram shows quantification of the effect of AVP. AVP significantly decreased the mean normalized sIPSC burst total area. Data are provided as mean ± SEM. A paired *t* test was used for statistical analysis.

Distinct spontaneous sharp wave events (SPWs), similar to those seen in mature rats and mice (32), were readily detected in LFP recordings from hippocampal slices of P0–P2 guinea pigs (Fig. 6*C*). In a manner similar to its action on fGDPs in the hippocampal preparation from perinatal rats, 10 nM AVP produced a pronounced suppression of neonatal guinea pig SPWs, which was prevented by SR49059 (20–30 nM) (Fig. 6*D*). Interneuronal activity is known to be crucial in shaping SPWs (32, 52, 53); hence, we examined whether the suppression of SPWs in the neonatal guinea pig was attributable to interneuronal activation by AVP. In whole-cell voltage-clamp recordings from CA3 pyramidal neurons, AVP induced a significant increase in sIPSC frequency, similar to that seen in rats (Fig. 6*E*). In sum, the present data demonstrate that AVP activates interneurons, and thereby suppresses perinatal hippocampal network events, regardless of whether the driving force for $GABA_AR$-mediated signaling is depolarizing or hyperpolarizing.

Discussion

The present study indicates that during birth, in parallel to peripheral AVP-mediated adaptive responses, such as those targeting the cardiorespiratory system (9), synergistic effects take place in the brain. Our data show that AVP has a powerful suppressive effect on perinatal hippocampal network events in species with altricial (rat) as well as precocial (guinea pig) neonates. It is indeed remarkable that in both species, the desynchronizing effect induced by AVP is similar, based on increased firing of interneurons, with an outcome at the network level that is not dependent on the stage of brain maturity at birth. We show that the present neurophysiological effects of AVP are based on V1aR-mediated signaling, which acts directly on neuronal network activity in a manner that is expected to have neuroprotective effects, as will be discussed below.

Tyzio et al. (40, 41) proposed a preemptively acting mechanism based on the actions of maternally derived OT, acting on OTRs in fetal hippocampal and neocortical pyramidal neurons to produce a large transient negative shift in E_{GABA}. In altricial species, a negative shift in E_{GABA} based on attenuation of secondary-active Cl^- uptake by NKCC1 would indeed be expected to reduce activity on the single-cell level as well as the network level (54), and consequently reduce the energy metabolic demand. However, our data show that in the rat hippocampus, $GABA_AR$ agonists have a constant depolarizing action on intact neurons from the late fetal (E21.5) to early postnatal period. We also show here that bumetanide-sensitive fGDPs were observed without exception in the intact rat hippocampus preparation as well as in acute hippocampal slices during the time window from E21.5 to postnatal hour 2 (PNH2) and later, matching our electrophysiological and imaging data on the depolarizing actions of perinatal GABA.

In numerous mammalian species, including humans, parturition is accompanied by a massive release of AVP by the fetus itself (reviewed in ref. 9). In the rat, AVP is detectable in the embryonic

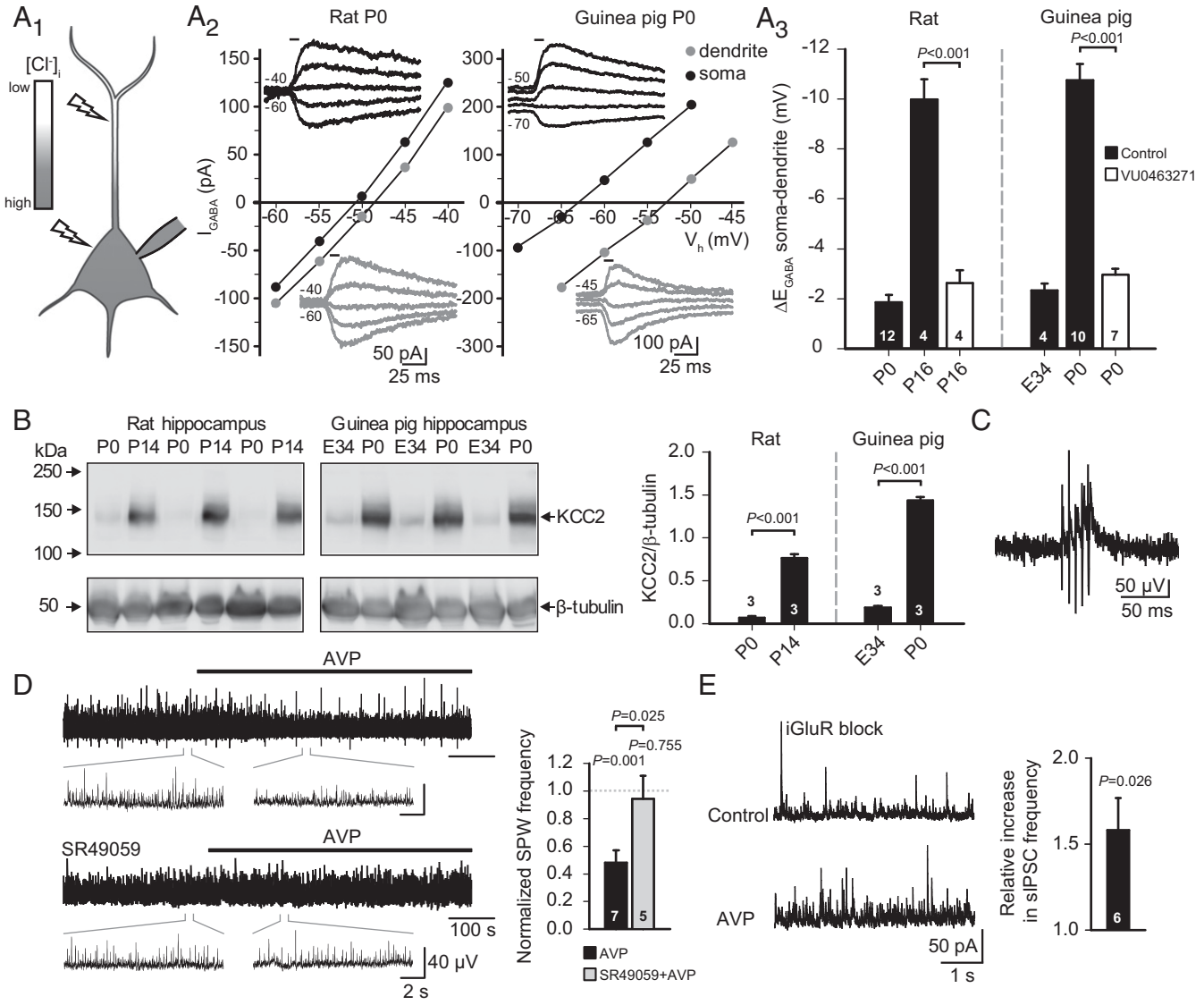

Fig. 6. AVP-mediated suppression of hippocampal network activity does not depend on the maturational level of neuronal Cl^- extrusion. (A_1) Scheme for quantitative assessment of neuronal Cl^- extrusion capacity from CA3 pyramidal neurons under a fixed somatic Cl^- load imposed via the patch pipette. Flashes illustrate the site of UV photolysis of caged GABA. (A_2 and A_3) Whole-cell patch-clamp recordings of GABA uncaging-elicited currents (I_{GABA}) in CA3 pyramidal neurons from P0 rat and P0 guinea pig with a somatically imposed Cl^- load. (A_2) Sample E_{GABA} recordings and corresponding current-voltage (I-V) curves at the soma and dendrite. Horizontal bars in the sample traces indicate the duration of the uncaging UV flash. (A_3) Cl^- extrusion capacity of CA3 pyramidal neurons from P0 and P16 rats, as well as from E34 and P0 guinea pigs, quantified as the mean somatodendritic E_{GABA} gradient. Some recordings were done in the presence of VU0463271 (10 μM), a specific KCC2 inhibitor. (*B*, *Left*) Western blot analysis of KCC2 expression in the hippocampus from the rat (P0 and P14) and guinea pig (E34 and P0). β-Tubulin was used as a loading control. (*B*, *Right*) Quantification of KCC2 protein levels. (*C*) LFP sample trace of P0 guinea pig CA3 SPW (filtered at 1–15 Hz). (*D*) LFP sample trace (*Left*, filtered at 1–15 Hz; magnification is shown in *Insets*) and quantification (*Right*) of the effect of AVP on SPW frequency, measured from the P0 guinea pig hippocampal CA3 region in the absence and presence of SR49059 (20–30 nM). (*E*) Effect of AVP on P0–P2 guinea pig sIPSC frequency. Sample traces of whole-cell voltage-clamp recordings (*Left*) and quantification of the mean increase in sIPSC frequency (*Right*) during bath application of AVP. Data are provided as mean ± SEM, and *n* values are provided in the figure. Paired and independent *t* tests were used for statistical analysis.

brain in its fully processed form already at E16 (55). In light of this, we hypothesized that a mechanism endogenous to the fetal brain could be an efficient strategy for neuroprotection during birth.

The idea that fetal AVP might have a neuromodulatory role during mammalian birth is supported by evidence for vasopressinergic innervation of the rat brain, including the hippocampus, already at late fetal stages (27). In agreement with this, our structural data based on CLARITY show that vasopressinergic innervation of the rat hippocampus is present at P0. Our electrophysiological data show that AVP at 10 nM suppressed fGDPs throughout the perinatal period, providing functional evidence of the neuromodulatory role of AVP. Notably, a shift in E_{GABA} was not the underlying mechanism of this suppression. Discrete events of synchronous network activity, such as GDPs and SPWs (32, 56), exert a particularly high energy-metabolic load on the brain due to the pronounced temporal coincidence of GABAergic and glutamatergic inputs (34). Hence, suppressing this synchronized activity would lead to a reduction of energy demand, which is highly beneficial under compromised conditions for oxygen supply, such as birth under normal, and especially pathophysiological, conditions, where intrapartum asphyxia is a prime example. Gross desynchronization of temporally structured activity, such as, for example, the AVP-mediated effect shown here, would be also very efficient to prevent the generation of

"nonsense" Hebbian associative synaptic connections in response to the extremely intense and unique sensory input that is associated with birth. A case in point here is the demonstration that GDPs act as coincidence detectors in the immature hippocampus to promote the development of functional connectivity (57, 58). Clearly, such an activity-dependent wiring mechanism would be blocked by AVP at birth, thereby directly suppressing the formation of maladaptive connectivity by birth-specific stimuli.

AVP is a potent modulator of interneurons and pyramidal neurons in the mature rat hippocampal CA1 area (59–62); however, comparable data from the developing hippocampus have not been reported. We now show enriched expression of V1aR mRNA in GABAergic interneurons in the CA3 region of the perinatal rat hippocampus, which, together with our electrophysiological data, suggests that interneurons are the main target of AVP in the perinatal rat CA3 region. It is well known that interneurons are important in the generation and shaping of network events and oscillations in the brain (32, 52, 53). Thus, an AVP-induced increase in the firing of hippocampal interneurons is expected to lead to the desynchronization and consequent suppression of fGDPs, as indeed was observed in the present study. With regard to the temporal properties of AVP actions, in our in vitro preparations, both the AVP-induced suppression of network events and the activation of interneurons were transient in nature, most likely due to receptor desensitization (45). When extrapolating these findings to in vivo conditions, it should be noted that AVP release from vasopressinergic fibers is triggered by bursts of action potentials (63); therefore, the desensitization seen with bath-applied AVP most likely has no counterpart in vivo.

The stage of brain development at birth shows enormous species-specific variation (51, 64, 65). With respect to birth, the timing of the developmental up-regulation of the main neuronal Cl^- extruder KCC2, and thus the shift from depolarizing to hyperpolarizing postsynaptic $GABA_AR$ signaling, is a pertinent example (30, 54, 66). We utilized the newborn guinea pig, a precocial rodent, in which cortical development is at a stage comparable to that of a 3-wk-old rat (65). The HPA axis and GABAergic mechanisms involved in the shaping of spontaneous network events are at a much more advanced level of development in the newborn guinea pig (10, 30), which makes the present comparisons between the rat and guinea pig uniquely valuable in identifying evolutionarily conserved mechanisms of mammalian neuroprotection at birth. In sharp contrast to rats, neonatal guinea pig hippocampal pyramidal neurons have a high capacity for KCC2-mediated Cl^- extrusion, which readily explains their hyperpolarizing $GABA_AR$ responses (30). In line with this, LFP recordings from neonatal guinea pig hippocampi displayed prominent SPWs, which closely resembled those seen in mature rats (32). As interneurons are essential in organizing pyramidal cell activity during SPWs (32, 52, 53), tonic interneuron spiking was expected to interfere with these network events. Indeed, as seen in the rat, AVP also enhanced interneuron firing in the guinea pig, which subsequently led to attenuation of SPWs. The fact that the effects of AVP showed basically similar characteristics in neonates of both the altricial rat and precocial guinea pig suggests a pan-mammalian protective action of AVP during birth. This implies that the present mechanism and conclusions are valid with regard to humans, where birth takes place at a stage of brain maturity that is intermediate with regard to the two rodent species examined.

In conclusion, an inadequate supply of oxygen associated with delivery under normal, and especially under pathophysiological, conditions is a major threat to the fetal mammalian brain. The obligatory period of asphyxia during the transition from umbilical cord-mediated to lung-based exchange of oxygen and carbon dioxide is known to be counteracted by hormonal and cardiovascular mechanisms leading to enhanced brain perfusion (1, 9). Our work indicates that in the fetal brain, AVP targets interneurons located in the hippocampus in a V1aR-dependent manner, leading to suppression of neuronal network activity, and thereby to a decrease in the activity-dependent energy demand (34). Given the high and widely recognized need for drugs that would protect the human neonate brain under adverse conditions, such as perinatal asphyxia (67), the present study may also open up avenues for the design of novel drugs that act on the vasopressinergic system.

Materials and Methods

Animals. Wistar rats [E21.5–P2 (perinatal), P14–P16, and P60] and guinea pigs (E34 ± 7 and P0–P2) of either sex were used for the study. PNH2 refers to rat pups, which have been decapitated within 15–120 min after birth. For targeted electrophysiological recordings from interneurons, VGAT-Venus transgenic rat pups of either sex (P0–P2) were used (48). All experiments carried out were approved by the National Animal Ethics Committee of Finland and the Local Animal Ethics Committee of the University of Helsinki.

Hippocampal Preparations. The preparation of acute horizontal brain slices (rat: 400–500 μm, guinea pig: 400–650 μm) and intact hippocampi (hippocampus in toto) was done as described previously (42, 68, 69). Details are provided in *Supporting Information*. Neonatal guinea pigs were deeply anesthetized with an i.p. injection of pentobarbital (~70 mg/kg) and transcardially perfused with ice-cold sucrose-based cutting solution before brain dissection. For collection of embryos, timed pregnant rats and guinea pigs were anesthetized (3–4% isoflurane), after which a cesarean section was performed and embryonic brains were collected in ice-cold cutting solution.

Intracellular Ca^{2+} Imaging. Intracellular Ca^{2+} imaging was done from acute hippocampal slices, which were loaded with Fluo-4-AM (Invitrogen/MolecularProbes). $GABA_AR$ activation was done by bath application of muscimol (5–10 μM; Tocris) or GABA (50–100 μM; Tocris) in the presence of TTX (1 μM, upon muscimol application) or TTX/CGP55845 (1 μM and 0.5 μM, respectively, upon GABA application). Details are provided in *Supporting Information*.

Electrophysiological Recordings. Electrophysiological recordings from acute slices and in toto preparations were performed in a submerged recording chamber at 32 ± 0.5 °C, constantly perfused with standard solution (3.5 $mL \cdot min^{-1}$ or 5 $mL \cdot min^{-1}$, respectively) in which the concentration of KCl was raised to 3.5–4 mM. Before recordings, preparations were equilibrating in the recording chamber for 15 min. Depending on the experiment, the following drugs were included in the extracellular solution: D-AP5 and CNQX [20 μM and 10 μM, respectively; Tocris (referred to as "iGluR block")], TTX (0.5 μM; Tocris), picrotoxin (100 μM; Tocris), and SR49059 (20–30 nM; Tocris).

LFP recordings were obtained with an EXT-02B amplifier (npi electronic GmbH) or a custom-made amplifier, using thin-filament glass-capillary electrodes with tip diameters of 5–10 μm, filled with 150 mM NaCl solution. The electrodes were placed in SP of the hippocampal CA3 area. Experiments were recorded to disk with WinEDR (Strathclyde Electrophysiology) using 1,000× gain and low-pass filtering at 1,000–5,000 Hz.

Whole-cell voltage-clamp and current-clamp recordings were obtained using an EPC 10 patch-clamp amplifier (HEKA) and recorded with Patchmaster (HEKA) at a sampling rate of 20–50 kHz. Borosilicate patch pipette resistance ranged from 3 to 8 MΩ. All cells included in the analyses had a resting membrane potential below −55 mV and a stable holding current. Series resistance compensation was performed online. Recordings in which the series resistance changed >25% or reached 25 MΩ were not included in the analysis. All voltages have been corrected for the respective liquid junction potential (LJP).

For CA3 pyramidal neuron excitability recordings in the loose cell-attached configuration, patch pipettes were filled with standard solution. Isoguvacine (100 μM, in standard solution) was puff-applied (50-ms puff duration) every 30 s from a glass capillary positioned over the slice, with the tip close to the soma of the recorded cell. The extracellular solution was supplemented with iGluR block throughout the recordings.

For whole-cell voltage-clamp recordings of IPSCs and EPSCs, the patch pipettes were filled with the following solution: 140 mM Cs-methanesulfonate, 2 mM $MgCl_2$, and 10 mM Hepes [with pH adjusted to 7.2 with CsOH (280 ± 5 mOsm), 13-mV calculated LJP]. For IPSC recordings, neurons were held at a holding potential of 0 mV (approximate equilibrium potential of glutamate receptor-mediated currents) and iGluR blockers were added to the extracellular solution when indicated. For mIPSC recordings, the extracellular solution was further supplemented with TTX. Due to high sIPSC frequencies in guinea pig

pyramidal neurons, only those recordings with a baseline sIPSC frequency below 25 Hz were analyzed. For EPSC recordings, neurons were held at a holding potential of −70 mV and picrotoxin was added to the extracellular solution.

For whole-cell current-clamp recordings (I = 0 pA) of spiking and membrane potential in pyramidal neurons and interneurons, the extracellular solution was supplemented with iGluR blockers and picrotoxin where indicated. Patch pipettes were filled with the following solution: 29 mM KCl, 101 mM K-gluconate, 0.5 mM $CaCl_2$, 5 mM 1,2-bis(2-aminophenoxy)ethane-*N*,*N*,*N*′,*N*′-tetraacetic acid (BAPTA), 10 mM Hepes, 10 mM glucose, 2 mM Mg-ATP, and 2 mM NaOH [with pH adjusted to 7.3 with KOH (280 ± 5 mOsm), and calculated LJP of 14 mV].

For quantitative assessment of neuronal Cl^- extrusion capacity, we used our standard assay, where a constant somatic Cl^- load (19 mM) is imposed on the neuron via a whole-cell patch pipette (70, 71). Details are provided in *Supporting Information*.

Analysis of Electrophysiological Recordings. The analysis of electrophysiological recordings was done with Clampfit (version 10.5; Axon). All clearly distinguishable fGDPs and GDP-associated sIPSC bursts were manually detected, and the area (megavolt × millisecond), which takes into account changes in both event amplitude and duration, was quantified using numerical integration in Clampfit for each event. Guinea pig SPWs were detected manually, using a threshold of 3× SD baseline noise. The event areas were assigned to 10-s bins according to the temporal occurrence of the events to obtain the total area for each bin. The data were normalized and presented as a moving average (60-s window, 10-s bins, 10-s step). IPSCs and sEPSCs were analyzed with Mini Analysis (Synaptosoft) using a threshold of three to four × baseline rms noise.

RNAscope in Situ Hybridization Assay. The detection of mRNA by RNAscope (Advanced Cell Diagnostics) was done according to the manual. Details are provided in *Supporting Information*. Specific probes to detect Gad1 (316401-C2), Gad2 (435801-C2), V1a (402531-C3), and V1b (443831) mRNA transcripts were designed and provided by Advanced Cell Diagnostics.

Western Blot. KCC2 protein levels in rat and guinea pig hippocampi were analyzed by Western blotting as described previously (72). Details are provided in *Supporting Information*.

CLARITY. CLARITY tissue was prepared as described by Tomer et al. (35), with minor modifications. Details are provided in *Supporting Information*.

Statistical Analysis. Independent or paired *t* tests were used to determine statistically significant differences between groups. All values are presented as mean ± SEM. Statistical significance was defined as $P < 0.05$. The effect of bath-applied neurohormones (AVP/OT) was quantified as the average within a 2-min time window starting 2 min after the beginning of application. The analysis was performed using IMB SPSS statistics 22.

ACKNOWLEDGMENTS. We thank Merle Kampura and Mairi Kuris for excellent technical assistance and Maria Partanen and Auli Kiukkonen for the maintaining and breeding of rats and guinea pigs. VGAT-Venus transgenic rats were generated by Drs. Y. Yanagawa, M. Hirabayashi, and Y. Kawaguchi (National Institute for Physiological Sciences, Okazaki, Japan), using pCS2-Venus provided by Dr. A. Miyawaki (RIKEN, Wako, Japan). The PS41 antibody was a generous gift from Dr. Harold Gainer (National Institute of Neurological Disorders and Stroke, NIH). This work was supported by Grant ERC-2013-AdG 341116 (to K.K.), and the Tarlton Foundation (K.D.).

1. Hillman NH, Kallapur SG, Jobe AH (2012) Physiology of transition from intrauterine to extrauterine life. *Clin Perinatol* 39:769–783.
2. Liu L, et al. (2015) Global, regional, and national causes of child mortality in 2000-13, with projections to inform post-2015 priorities: An updated systematic analysis. *Lancet* 385:430–440.
3. Ahearne CE, Boylan GB, Murray DM (2016) Short and long term prognosis in perinatal asphyxia: An update. *World J Clin Pediatr* 5:67–74.
4. Kikkawa Y, Kaibara M, Motoyama EK, Orzalesi MM, Cook CD (1971) Morphologic development of fetal rabbit lung and its acceleration with cortisol. *Am J Pathol* 64: 423–442.
5. Motoyama EK, et al. (1971) Effect of cortisol on the maturation of fetal rabbit lungs. *Pediatrics* 48:547–555.
6. Liggins GC (1994) The role of cortisol in preparing the fetus for birth. *Reprod Fertil Dev* 6:141–150.
7. Fowden AL, Li J, Forhead AJ (1998) Glucocorticoids and the preparation for life after birth: Are there long-term consequences of the life insurance? *Proc Nutr Soc* 57:113–122.
8. Crossley KJ, et al. (2009) Antenatal corticosteroids increase fetal, but not postnatal, pulmonary blood flow in sheep. *Pediatr Res* 66:283–288.
9. Evers KS, Wellmann S (2016) Arginine vasopressin and copeptin in perinatology. *Front Pediatr* 4:75.
10. Kapoor A, Dunn E, Kostaki A, Andrews MH, Matthews SG (2006) Fetal programming of hypothalamo-pituitary-adrenal function: Prenatal stress and glucocorticoids. *J Physiol* 572:31–44.
11. Buijs RM, Swaab DF, Dogterom J, van Leeuwen FW (1978) Intra- and extra-hypothalamic vasopressin and oxytocin pathways in the rat. *Cell Tissue Res* 186: 423–433.
12. Hou-Yu A, Lamme AT, Zimmerman EA, Silverman AJ (1986) Comparative distribution of vasopressin and oxytocin neurons in the rat brain using a double-label procedure. *Neuroendocrinology* 44:235–246.
13. Wellmann S, et al. (2010) High copeptin concentrations in umbilical cord blood after vaginal delivery and birth acidosis. *J Clin Endocrinol Metab* 95:5091–5096.
14. Schlapbach LJ, et al. (2011) Copeptin concentration in cord blood in infants with early-onset sepsis, chorioamnionitis and perinatal asphyxia. *BMC Pediatr* 11:38.
15. Hoppenstein JM, Miltenberger FW, Moran WH, Jr (1968) The increase in blood levels of vasopressin in infants during birth and surgical procedures. *Surg Gynecol Obstet* 127:966–974.
16. Chard T, Hudson CN, Edwards CR, Boyd NR (1971) Release of oxytocin and vasopressin by the human foetus during labour. *Nature* 234:352–354.
17. Polin RA, Husain MK, James LS, Frantz AG (1977) High vasopressin concentrations in human umbilical cord blood–Lack of correlation with stress. *J Perinat Med* 5:114–119.
18. Summanen M, et al. (2017) Comparison of umbilical serum copeptin relative to erythropoietin and S100B as asphyxia biomarkers at birth. *Neonatology* 112:60–66.
19. Kendrick KM, Keverne EB, Hinton MR, Goode JA (1991) Cerebrospinal fluid and plasma concentrations of oxytocin and vasopressin during parturition and vaginocervical stimulation in the sheep. *Brain Res Bull* 26:803–807.
20. Bartrons J, Figueras J, Jiménez R, Gaya J, Cruz M (1993) Vasopressin in cerebrospinal fluid of newborns with hypoxic-ischemic encephalopathy. Preliminary report. *J Perinat Med* 21:399–403.
21. Carson DS, et al. (2014) Plasma vasopressin concentrations positively predict cerebrospinal fluid vasopressin concentrations in human neonates. *Peptides* 61:12–16.
22. Ruth V, Fyhrquist F, Clemons G, Raivio KO (1988) Cord plasma vasopressin, erythropoietin, and hypoxanthine as indices of asphyxia at birth. *Pediatr Res* 24:490–494.
23. Tang LQ, Ringstedt T, Pequignot J, Lagercrantz H (2000) C-fos gene expression in rat brain around birth: Effect of asphyxia and catecholamines. *Brain Res* 852:84–91.
24. Buijs RM, Velis DN, Swaab DF (1980) Extrahypothalamic vasopressin and oxytocin innervation of fetal and adult rat brain. *Prog Brain Res* 53:159–167.
25. Rood BD, De Vries GJ (2011) Vasopressin innervation of the mouse (Mus musculus) brain and spinal cord. *J Comp Neurol* 519:2434–2474.
26. Zhang L, Hernández VS (2013) Synaptic innervation to rat hippocampus by vasopressin-immuno-positive fibres from the hypothalamic supraoptic and paraventricular nuclei. *Neuroscience* 228:139–162.
27. Buijs RM, Velis DN, Swaab DF (1980) Ontogeny of vasopressin and oxytocin in the fetal rat: Early vasopressinergic innervation of the fetal brain. *Peptides* 1:315–324.
28. Zhao L, Brinton RD (2004) Suppression of proinflammatory cytokines interleukin-1beta and tumor necrosis factor-alpha in astrocytes by a V1 vasopressin receptor agonist: A cAMP response element-binding protein-dependent mechanism. *J Neurosci* 24: 2226–2235.
29. Chen J, Aguilera G (2010) Vasopressin protects hippocampal neurones in culture against nutrient deprivation or glutamate-induced apoptosis. *J Neuroendocrinol* 22: 1072–1081.
30. Rivera C, et al. (1999) The K+/Cl- co-transporter KCC2 renders GABA hyperpolarizing during neuronal maturation. *Nature* 397:251–255.
31. Sipilä ST, Huttu K, Soltesz I, Voipio J, Kaila K (2005) Depolarizing GABA acts on intrinsically bursting pyramidal neurons to drive giant depolarizing potentials in the immature hippocampus. *J Neurosci* 25:5280–5289.
32. Buzsáki G (2015) Hippocampal sharp wave-ripple: A cognitive biomarker for episodic memory and planning. *Hippocampus* 25:1073–1188.
33. Wester JC, McBain CJ (2016) Interneurons differentially contribute to spontaneous network activity in the developing hippocampus dependent on their embryonic lineage. *J Neurosci* 36:2646–2662.
34. Buzsáki G, Kaila K, Raichle M (2007) Inhibition and brain work. *Neuron* 56:771–783.
35. Tomer R, Ye L, Hsueh B, Deisseroth K (2014) Advanced CLARITY for rapid and high-resolution imaging of intact tissues. *Nat Protoc* 9:1682–1697.
36. Ben-Barak Y, Russell JT, Whitnall MH, Ozato K, Gainer H (1985) Neurophysin in the hypothalamo-neurohypophysial system. I. Production and characterization of monoclonal antibodies. *J Neurosci* 5:81–97.
37. Stoop R (2012) Neuromodulation by oxytocin and vasopressin. *Neuron* 76:142–159.
38. Ben-Ari Y, Gaiarsa JL, Tyzio R, Khazipov R (2007) GABA: A pioneer transmitter that excites immature neurons and generates primitive oscillations. *Physiol Rev* 87: 1215–1284.
39. Ben-Ari Y, Cherubini E, Corradetti R, Gaiarsa JL (1989) Giant synaptic potentials in immature rat CA3 hippocampal neurones. *J Physiol* 416:303–325.
40. Tyzio R, et al. (2006) Maternal oxytocin triggers a transient inhibitory switch in GABA signaling in the fetal brain during delivery. *Science* 314:1788–1792.
41. Tyzio R, et al. (2014) Oxytocin-mediated GABA inhibition during delivery attenuates autism pathogenesis in rodent offspring. *Science* 343:675–679.
42. Khalilov I, et al. (1997) A novel in vitro preparation: The intact hippocampal formation. *Neuron* 19:743–749.
43. Kirmse K, et al. (2015) GABA depolarizes immature neurons and inhibits network activity in the neonatal neocortex in vivo. *Nat Commun* 6:7750.

44. Valeeva G, Tressard T, Mukhtarov M, Baude A, Khazipov R (2016) An optogenetic approach for investigation of excitatory and inhibitory network GABA actions in mice expressing channelrhodopsin-2 in GABAergic neurons. *J Neurosci* 36:5961–5973.
45. Birnbaumer M (2000) Vasopressin receptors. *Trends Endocrinol Metab* 11:406–410.
46. Manning M, et al. (2012) Oxytocin and vasopressin agonists and antagonists as research tools and potential therapeutics. *J Neuroendocrinol* 24:609–628.
47. Serradeil-Le Gal C, et al. (1993) Biochemical and pharmacological properties of SR 49059, a new, potent, nonpeptide antagonist of rat and human vasopressin V1a receptors. *J Clin Invest* 92:224–231.
48. Uematsu M, et al. (2008) Quantitative chemical composition of cortical GABAergic neurons revealed in transgenic venus-expressing rats. *Cereb Cortex* 18:315–330.
49. Wang F, et al. (2012) RNAscope: A novel in situ RNA analysis platform for formalin-fixed, paraffin-embedded tissues. *J Mol Diagn* 14:22–29.
50. Khazipov R, Leinekugel X, Khalilov I, Gaiarsa JL, Ben-Ari Y (1997) Synchronization of GABAergic interneuronal network in CA3 subfield of neonatal rat hippocampal slices. *J Physiol* 498:763–772.
51. Erecinska M, Cherian S, Silver IA (2004) Energy metabolism in mammalian brain during development. *Prog Neurobiol* 73:397–445.
52. McBain CJ, Fisahn A (2001) Interneurons unbound. *Nat Rev Neurosci* 2:11–23.
53. Klausberger T, Somogyi P (2008) Neuronal diversity and temporal dynamics: The unity of hippocampal circuit operations. *Science* 321:53–57.
54. Kaila K, Price TJ, Payne JA, Puskarjov M, Voipio J (2014) Cation-chloride cotransporters in neuronal development, plasticity and disease. *Nat Rev Neurosci* 15:637–654.
55. Altstein M, Gainer H (1988) Differential biosynthesis and posttranslational processing of vasopressin and oxytocin in rat brain during embryonic and postnatal development. *J Neurosci* 8:3967–3977.
56. Leinekugel X, et al. (2002) Correlated bursts of activity in the neonatal hippocampus in vivo. *Science* 296:2049–2052.
57. Mohajerani MH, Sivakumaran S, Zacchi P, Aguilera P, Cherubini E (2007) Correlated network activity enhances synaptic efficacy via BDNF and the ERK pathway at immature CA3 CA1 connections in the hippocampus. *Proc Natl Acad Sci USA* 104:13176–13181.
58. Kasyanov AM, Safiulina VF, Voronin LL, Cherubini E (2004) GABA-mediated giant depolarizing potentials as coincidence detectors for enhancing synaptic efficacy in the developing hippocampus. *Proc Natl Acad Sci USA* 101:3967–3972.
59. Tiberiis BE, McLennan H, Wilson N (1983) Neurohypophysial peptides and the hippocampus. II. Excitation of rat hippocampal neurones by oxytocin and vasopressin applied in vitro. *Neuropeptides* 4:73–86.
60. Mizuno Y, Oomura Y, Hori N, Carpenter DO (1984) Action of vasopressin on CA1 pyramidal neurons in rat hippocampal slices. *Brain Res* 309:241–246.
61. Mühlethaler M, Charpak S, Dreifuss JJ (1984) Contrasting effects of neurohypophysial peptides on pyramidal and non-pyramidal neurones in the rat hippocampus. *Brain Res* 308:97–107.
62. Ramanathan G, et al. (2012) Vasopressin facilitates GABAergic transmission in rat hippocampus via activation of V(1A) receptors. *Neuropharmacology* 63:1218–1226.
63. Wakerley JB, Poulain DA, Brown D (1978) Comparison of firing patterns in oxytocin- and vasopressin-releasing neurones during progressive dehydration. *Brain Res* 148: 425–440.
64. Dobbing J, Sands J (1979) Comparative aspects of the brain growth spurt. *Early Hum Dev* 3:79–83.
65. Clancy B, Darlington RB, Finlay BL (2001) Translating developmental time across mammalian species. *Neuroscience* 105:7–17.
66. Sedmak G, et al. (2016) Developmental expression patterns of KCC2 and functionally associated molecules in the human brain. *Cereb Cortex* 26:4574–4589.
67. Donovan MD, Griffin BT, Kharoshankaya L, Cryan JF, Boylan GB (2016) Pharmacotherapy for neonatal seizures: Current knowledge and future perspectives. *Drugs* 76: 647–661.
68. Valeeva G, Valiullina F, Khazipov R (2013) Excitatory actions of GABA in the intact neonatal rodent hippocampus in vitro. *Front Cell Neurosci* 7:20.
69. Puskarjov M, Ahmad F, Kaila K, Blaesse P (2012) Activity-dependent cleavage of the K-Cl cotransporter KCC2 mediated by calcium-activated protease calpain. *J Neurosci* 32:11356–11364.
70. Khirug S, et al. (2005) Distinct properties of functional KCC2 expression in immature mouse hippocampal neurons in culture and in acute slices. *Eur J Neurosci* 21:899–904.
71. Puskarjov M, et al. (2015) BDNF is required for seizure-induced but not developmental up-regulation of KCC2 in the neonatal hippocampus. *Neuropharmacology* 88: 103–109.
72. Uvarov P, et al. (2009) Coexpression and heteromerization of two neuronal K-Cl cotransporter isoforms in neonatal brain. *J Biol Chem* 284:13696–13704.